Black Arsenic–Phosphorus: Layered Anisotropic Infrared Semiconductors with Highly Tunable Compositions and Properties

*Bilu Liu, Marianne Köpf, Ahmad N. Abbas, Xiaomu Wang, Qiushi Guo, Yichen Jia, Fengnian Xia, Richard Weihrich, Frederik Bachhuber, Florian Pielnhofer, Han Wang, Rohan Dhall, Stephen B. Cronin, Mingyuan Ge, Xin Fang, Tom Nilges, and Chongwu Zhou**

In recent years, 2D layered materials, including graphene,[1–3] hexagonal boron nitride (h-BN),[4–6] transition metal dichalcogenides (TMDCs),[7–12] and black phosphorus (b-P),[13–19] have attracted significant interest due to their unique electronic, optical, and mechanical properties. To date, these 2D layered materials have covered a wide electromagnetic spectral range including metals, semimetals, semiconductors, and insulators. Specifically, monolayer graphene is a semimetal which exhibits a zero band gap in its natural state and strong electrical field can be used in order to create a band gap in bilayer graphene.[20] On the other end of the spectrum, h-BN is an insulator with a large band gap of around 6 eV, which extends into the middle ultraviolent regime. TMDCs have a formula of MX_2, where M is a transition metal element and X is a chalcogen element. TMDCs can be either metals or semiconductors, depending on the transition elements.[21] The most heavily studied TMDCs so far (M = Mo or W, and X = S, Se, or Te) possess band gaps in the range from around 1.0 to 1.9 eV via tuning the chemical compositions, layer numbers, and strains of the materials.[21–26] These TMDC materials fill up part of the gap between graphene and h-BN in the electromagnetic spectra. One of the newest members of the 2D layered material family is b-P,[13–16] which is a semiconductor exhibiting a moderate band gap of around 0.3 eV in its bulk form and up to 2.2 eV as in a monolayer,[27] further pushing the band gap of layered materials to the middle-wavelength infrared regime (MWIR, 0.3 eV corresponds to a wavelength of 4.13 μm). Therefore, a broad spectral range has now been covered by the above-mentioned layered materials. Nevertheless, there is a technologically important wavelength range, the long-wavelength infrared (LWIR) regime, which still cannot be readily covered by the 2D layered materials mentioned above. This particular electromagnetic spectral range is important for a range of applications such as range finding using LIDAR (light radar) systems because the earth atmosphere (mostly H_2O, O_3, and CO_2) has good transparency in this spectral range (starting at around 8 μm). Therefore, new layered semiconducting materials that cover this distinct electromagnetic spectral range are desirable for the realization of devices and systems based on all 2D layered materials.

Alloying is a general strategy that has been used for tuning the properties of materials for thousands of years. Graphene, BN, and TMDCs with tunable properties can be synthesized via such alloying or doping methods.[6,23,25,26] It has been shown two decades ago that arsenic can be incorporated into b-P via a high pressure process, and these materials show superconducting properties at around 10 K.[28] Here, we introduce a family of layered semiconductors, black arsenic–phosphorus (b-AsP), via a new synthetic approach adopting the alloying strategy. Our method involves the synthesis of layered b-AsP materials with different and tunable compositions (b-As_xP_{1-x}, with x in the range of 0–0.83), using a novel mineralizer-assisted short way chemical transport reaction (see the Experimental Section). More importantly, thanks to the good tunability of the chemical compositions, we demonstrate that these layered b-AsP materials have fully tunable band gaps and optical properties that cover long wavelengths down to around 0.15 eV (corresponds to a wavelength of 8.27 μm, LWIR regime).

A new synthetic route is used for the synthesis of b-AsP in this study, which uses ultrapure gray arsenic and red phosphorus as starting materials. This new route was developed based on our earlier work [29,30] and inspired by the work on the synthesis of b-P.[17,31,32] The as-synthesized materials are black shin flakes or needle-like structures. X-ray diffraction (Figure S1, Supporting Information)[30] and transmission electron microscopy (Figure S2, Supporting Information) characterization shows that this family of layered b-AsP materials, similar to b-P, have orthorhombic structure with a puckered

Dr. B. Liu, A. N. Abbas, Prof. H. Wang, R. Dhall, Prof. S. B. Cronin, M. Ge, X. Fang, Prof. C. Zhou
Ming Hsieh Department of Electrical Engineering
University of Southern California
Los Angeles, CA 90089, USA
E-mail: chongwuz@usc.edu

M. Köpf, Prof. T. Nilges
Department of Chemistry
Technische Universität München
Lichtenbergstraße 4, Garching b, München 485748, Germany

Dr. X. Wang, Q. Guo, Y. Jia, Prof. F. Xia
Department of Electrical Engineering
Yale University
New Haven, CT 06511, USA

Prof. R. Weihrich, F. Bachhuber, F. Pielnhofer
Institut für Anorganische Chemie
Universität Regensburg, Universitätsstraße 31
Regensburg 93040, Germany

DOI: 10.1002/adma.201501758

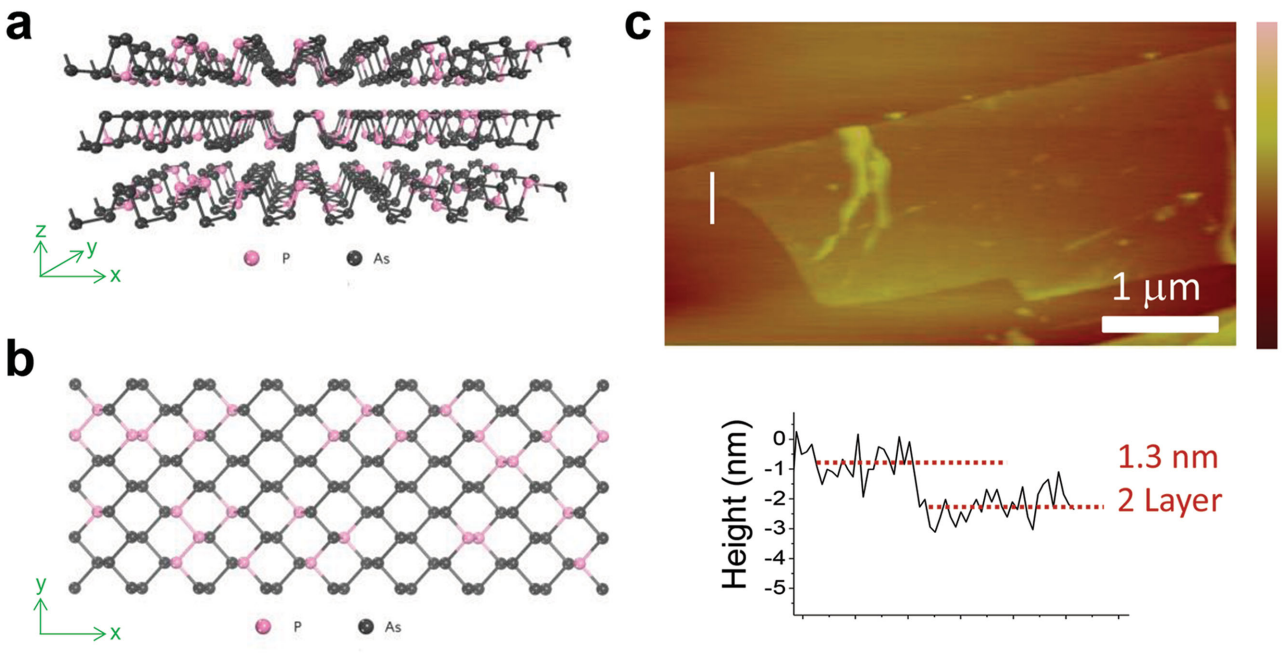

Figure 1. Structure and exfoliation of layered b-AsP. a) Side view and b) top view of b-AsP. This family of layered materials has orthorhombic lattice with puckered honeycomb structure (A17 type). The arsenic and phosphorus atoms are distributed within each layer and their concentrations are tunable. c) An AFM image of an exfoliated bilayer b-$As_{0.83}P_{0.17}$ flake with a thickness of ≈1.3 nm.

honeycomb lattice (A17 type structure, see **Figure 1**a,b). Arsenic and phosphorus atoms are distributed in the materials and the volume of the unit cell increases with increasing arsenic content (Figure S3, Supporting Information). Therefore, these b-AsP materials have strong in-plane covalent bonding and weak interlayer van der Walls interactions, sharing the common features with many other layered 2D materials.

These layered b-AsP materials can be mechanically exfoliated into thin flakes down to atomic layers. Figure 1c shows an atomic-force microscopy (AFM) image of a b-$As_{0.83}P_{0.17}$ flake with a thickness of 1.3 nm, corresponding to two atomic layers. Interestingly, during exfoliation experiments, we found that the difficulty in exfoliating these materials increases as the arsenic content increases in the b-AsP materials; an indication of the enhanced interlayer interaction for materials with high arsenic content. This phenomenon may shed light on future studies of the strength of interlayer van der Walls interactions in layered materials of group V elements.

To study the charge transport properties in these materials, we fabricated back-gate field-effect transistors (FETs) using exfoliated b-$As_{0.83}P_{0.17}$ flakes as channel materials. The samples were exfoliated onto Si substrates covered with 300 nm SiO_2 layer and the devices were fabricated using e-beam lithography. The metal contact was Ti/Au with thickness of 1/50 nm or 5/50 nm. **Figure 2**a shows a 3D AFM image of a typical b-AsP FET, which possesses a channel length of 1.3 μm and a channel width of 2 μm. We found that for thick b-AsP samples (>20–30 nm in thickness), the devices are highly conductive and exhibit very weak gate dependence due to screening effect (see Figure S4 in the Supporting Information). When the flakes become thin, increased gate modulation to the channel conductance was observed. Figure 2b shows the transfer curves of a 15 nm thick b-$As_{0.83}P_{0.17}$ flake at different bias voltages. This device shows a hole mobility of 110 $cm^2\ V^{-1}\ s^{-1}$ under two-terminal configuration. Figure 2c shows transfer curve of a thin (5 nm) b-$As_{0.83}P_{0.17}$ flake. This device shows ambipolar transport behavior and an on/off current ratio of 1.9×10^3. These transport measurements reveal the semiconducting nature of b-AsP materials.

One major motivation of studying layered b-AsP materials is whether we can tune the band gaps of these materials by tuning the chemical compositions. We used polarization-resolved infrared absorption spectroscopy to measure the band gaps as well as anisotropic behavior of b-AsP. **Figure 3**a shows infrared absorption spectra of b-$As_{0.83}P_{0.17}$, which has the highest arsenic content in this study. The results show that this material has an absorption edge of around 1250 cm^{-1}, corresponding to a band gap of 0.15 eV. Noticeably, this band gap is only half of the band gap of b-P (around 0.3 eV) and reaches the LWIR regime. Moreover, the polarization-resolved infrared absorption spectra clearly show the anisotropic absorption behavior of b-$As_{0.83}P_{0.17}$ (Figure 3a). A full list of polarization-resolved spectra with an angle step of 15° are shown in Figure S5 (Supporting Information), and for clarity, only four spectra are shown in Figure 3a. Quantitative analysis of the absorption intensity at 2200 cm^{-1} is exhibited in Figure 3b. The absorption maximum is found at an angle of 135°, which is close to the *x*-axis of the flake (see Figure 1a,b) with an error of less than 7.5° (due to the use of 15° angle step during experiments). Accordingly, the absorption minimum is located at an angle of 45°, with is close to the *y*-axis of the flake.

We performed systematic polarization-resolved infrared absorption studies on a family of b-As_xP_{1-x} with different *x* values of 0, 0.25, 0.4, and 0.83. Figure 3c shows a collection

Adv. Mater. **2015**,
DOI: 10.1002/adma.201501758

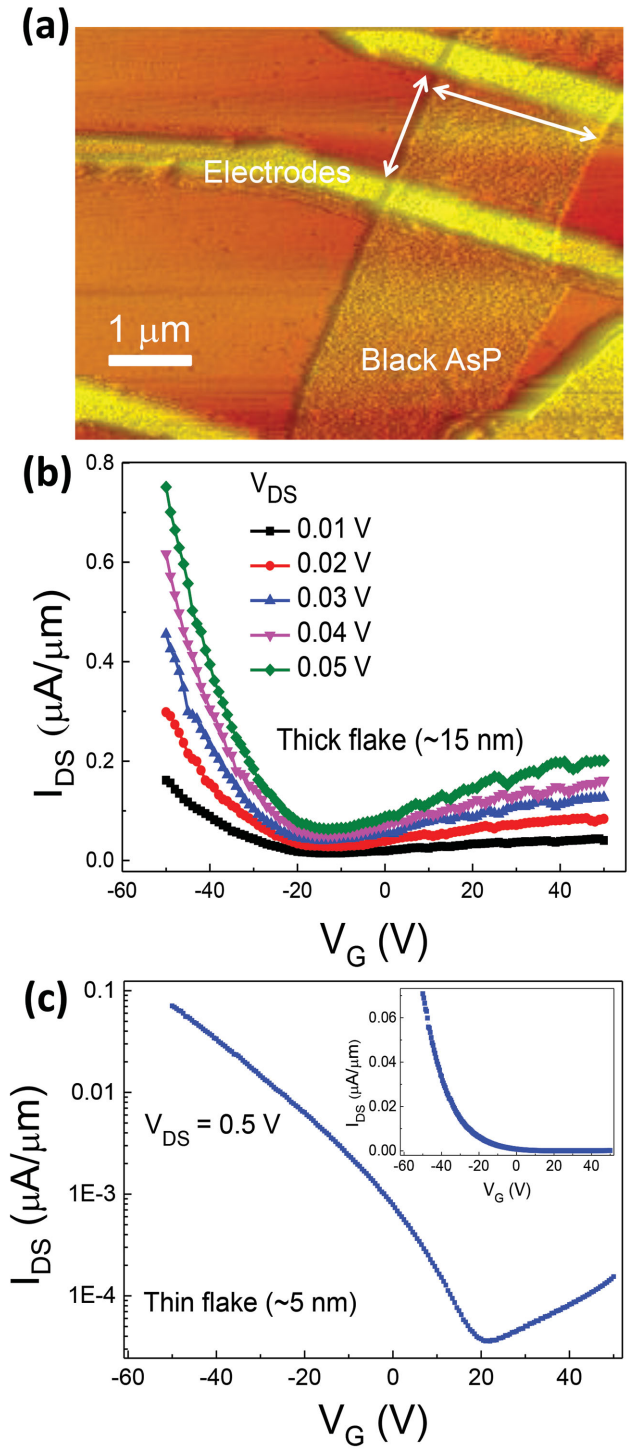

Figure 2. FET of back-gate black arsenic–phosphorus. a) An AFM image of a b-AsP FET. The channel length and width of the device are 1.3 and 2 μm as highlighted using white arrows. b) Transfer curves of a representative thick b-$As_{0.83}P_{0.17}$ flake. The thickness of the flake is around 15 nm and the hole mobility of this device is 110 $cm^2 V^{-1} s^{-1}$. c) Transfer curve of a thin b-$As_{0.83}P_{0.17}$ flake in semilog scale and linear scale (inset). The device shows am-bipolar behavior and an on/off current ratio of 1.9×10^3 at hole side (p-branch). The thickness of the flake is around 5 nm. The substrates are Si/SiO_2 (300 nm).

of infrared absorption spectra for b-AsP with different compositions. A clear shift of the absorption edges to shorter wavelengths with increasing x in b-As_xP_{1-x} is observed, confirming that the band gaps of b-As_xP_{1-x} change with the chemical composition of the material. This result provides the basis for applications of these layered b-AsP materials in a variety of fields including electronics and optoelectronics, such as middle to long-wavelength infrared photodetection and optical imaging.

We have conducted infrared absorption measurements on these materials and collected a total of around 80 spectra for statistical analysis. Figure 3d shows a summary of the results based on multiple spectra taken for each composition. It should be noted that all the flakes measured in Figure 3d are relatively thick ones with thicknesses greater than 30 nm. One can clearly see that the band gaps decrease with increasing arsenic content in the b-As_xP_{1-x} materials. Noticeably, the band gaps of these layered b-As_xP_{1-x} materials can be fully tuned over the range from 0.3 eV (in the case of b-As_0P_1, i.e., pure b-P) to 0.15 eV (in b-$As_{0.83}P_{0.17}$). Further increasing the arsenic content, for example, up to pure black arsenic (b-As, here we refer to orthorhombic structure arsenic, A17 type structure), may push the band gap to the even longer wavelength regime. Recent revPBE-van der Waals calculations show that pure b-As is a metal with zero band gap in bulk and exhibits high charge carrier mobilities in few layer form.[33] So far, there has been no success in the synthesis of pure b-As due to its metastability and the lack of suitable synthesis strategies.[30] We note that due to the applied short way vapor transport reaction, a variation of the composition within one sample is possible. We have crosschecked multiple crystals of each batch by energy-dispersive X-ray spectroscopy (EDX) and found that the contents of arsenic and phosphorus (As/P ratio) fall into a reasonably narrow range. Therefore, a small variation of composition of the materials does not change the big picture of composition-dependent band gaps we reported in this study.

Interestingly, one can discern from Figure 3d that the band gaps of the b-As_xP_{1-x} decrease sharply when the arsenic content changed from 0 to 0.25 and then decrease less significantly when the arsenic content changes from 0.25 to 0.4 and further to 0.83. The results suggest that the band gaps do not scale linearly with the content of arsenic or phosphorus. The general trend of composition-dependent band gaps obtained from infrared absorption measurements shows agreement with our density-functional theory (DFT) calculations shown in Table S1 (Supporting Information).

We have further substantiated the anisotropic properties of these b-As_xP_{1-x} materials via polarization-resolved Raman spectroscopy studies. Here, we use b-$As_{0.83}P_{0.17}$ as an example to present this behavior. In our experiments, light is linearly incident from the z-direction, is polarized in the x–y plane, and the detection is in the z-direction and unpolarized. The wavelength of laser is 532 nm and the spot size is ≈1 μm. We first compared the Raman spectra of b-$As_{0.83}P_{0.17}$ with pure b-P and b-As. For b-As, since there have been no reports on the synthesis and Raman characterization of this material so far, we therefore calculated its Raman spectra. It can be seen that the characteristic peaks of these systems are quite different

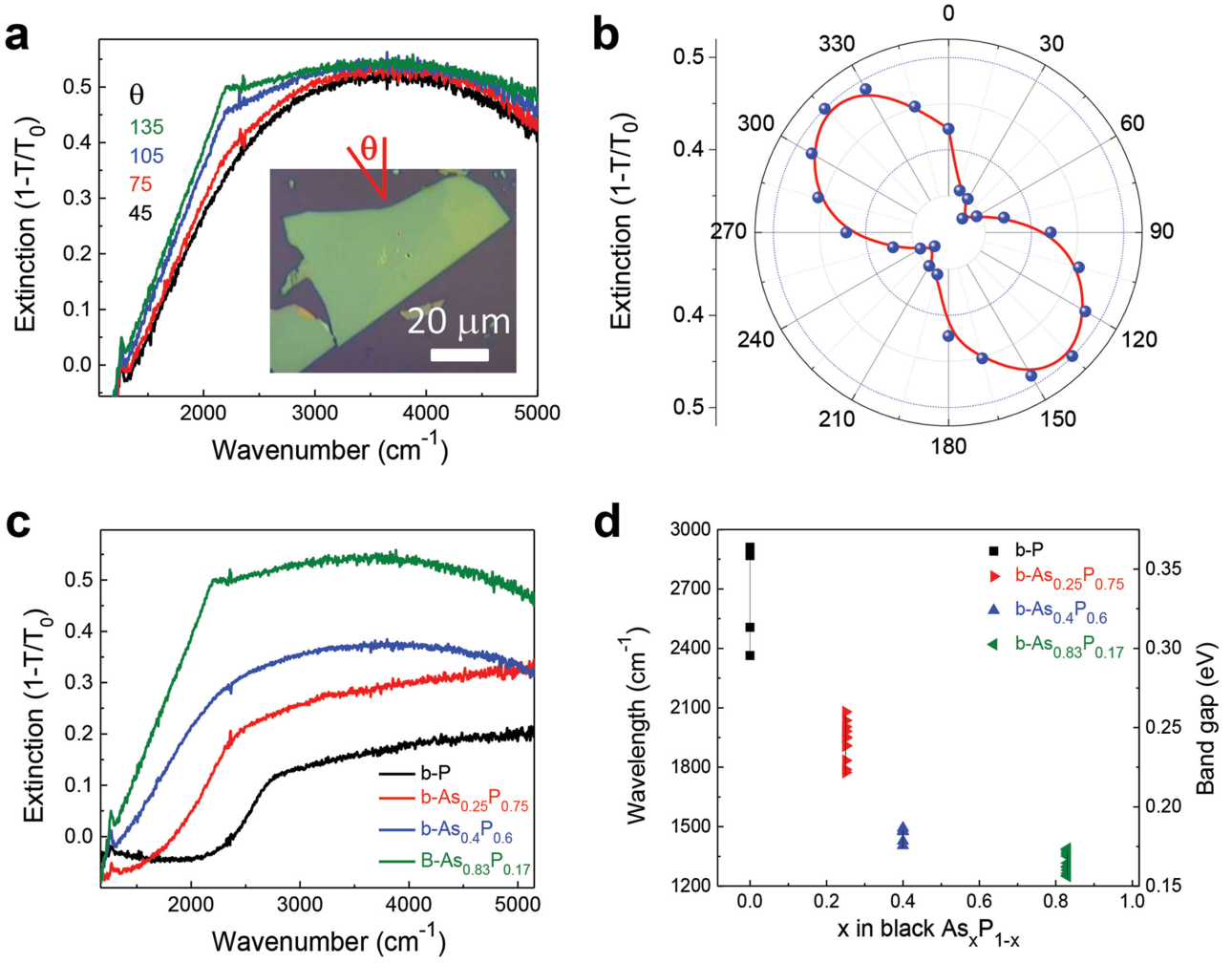

Figure 3. Anisotropic layered black arsenic–phosphorus semiconductors with tunable electronic and optical properties. a) Polarization-resolved infrared absorption spectra of b-$As_{0.83}P_{0.17}$ materials at different polarization angles, showing clearly polarization-dependent absorption behavior. The inset is the optical microscopy image of the flake and the polarization angle indication. The thickness of this flake is 122 nm based on AFM measurements. For clarify, only four curves with angles of 45°, 75°, 105°, and 135° were shown. A collection of all 13 spectra from 0° to 165° are shown in Figure S5 (Supporting Information). b) Dependence of the extinction intensity at 2200 cm^{-1} with polarization angles. c) Plots of infrared absorption of different b-As_xP_{1-x} samples, showing the involution of band gaps with tuning *x* in b-As_xP_{1-x} materials. The *x* is the nominal composition of arsenic, which corresponds to 0, 0.25, 0.40, and 0.83 in this work. Note that the absolute extinction values of the spectra in plot c cannot be compared directly, since the flake thicknesses and sizes are different for different samples. d) Summary of *x*-dependent band gaps of b-As_xP_{1-x}. Each data point corresponds to a measurement from either different polarization angle of the same flake or from different flakes of the same composition. The thickness of the b-AsP flakes is >30 nm in these IR measurements.

(Figures S6 and S7, and Table S2, Supporting Information), indicating different vibrational properties. The Raman spectra of b-P have been well documented, and three major peaks are observed, including the out-of-plane A_g^1 peak at 363 cm^{-1}, the in-plane B_{2g} peak at 440 cm^{-1}, and the in-plane A_g^2 peak at 467 cm^{-1}. These experimental observations are consistent with our calculations (Figure S7 and Table S2, Supporting Information) and recent reports on the Raman spectra of b-P.[13–16,27] For b-As, our calculations indicate the A_g^1 peak at 237 cm^{-1}, the B_{2g} peak at 241 cm^{-1}, and the A_g^2 peak at 273 cm^{-1} (Figure S7 and Table S2, Supporting Information).

As a contrast, b-$As_{0.83}P_{0.17}$ exhibits more Raman peaks (**Figures 4**a and S5, Supporting Information) than both b-P and b-As, in good accordance with the occurrence of heteroatomic arsenic-phosphorus bonds. One can see that the Raman spectra of b-$As_{0.83}P_{0.17}$ can be divided into three major regimes, low frequency (≈200–300 cm^{-1}), medium frequency (≈300–380 cm^{-1}), and high frequency (≈380–500 cm^{-1}) regimes. Dependent on the grade of substitution of phosphorus by arsenic, we observed that the relative intensity of peaks at each regime varies significantly. Specifically for b-$As_{0.83}P_{0.17}$, the three peaks from low frequency regime (≈200–300 cm^{-1}), i.e., 224, 233, and 256 cm^{-1}, dominate the spectra. We have assigned these peaks to A_g^1, B_{2g}, and A_g^2 modes of b-$As_{0.83}P_{0.17}$. There are systematical blueshifts in peak positions compared with our calculated data on pure b-As (Table S2, Supporting Information), because the existence of phosphorus atoms in b-$As_{0.83}P_{0.17}$ can blueshift the Raman peaks of b-As. With increasing the phosphorus content,

Adv. Mater. **2015**,
DOI: 10.1002/adma.201501758

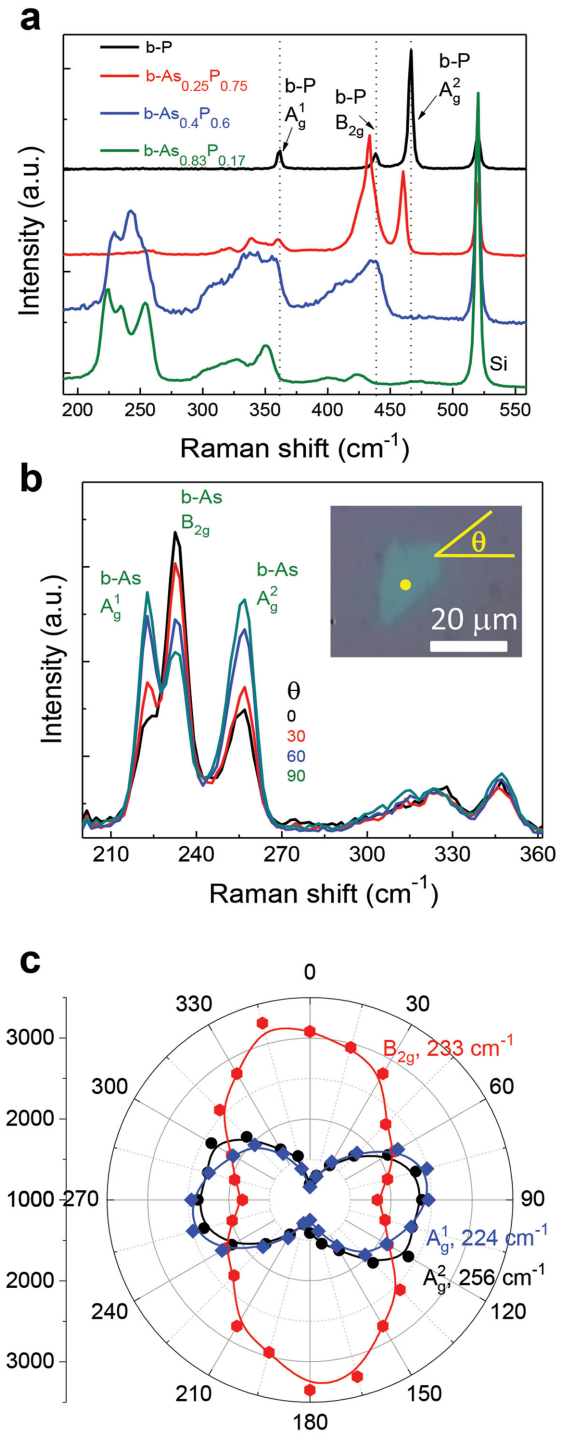

Figure 4. Polarization-resolved micro-Raman spectroscopic characterization of b-$As_{0.83}P_{0.17}$. a) Raman spectra of b-AsP with different chemical compositions, showing the evolution of Raman peaks with changing arsenic content. b) Polarization-dependent Raman spectra of a b-$As_{0.83}P_{0.17}$ sample at different polarization angles of 0°, 30°, 60°, and 90°. Clear polarization-dependent Raman intensities can be discerned. The inset is the optical microscopy image of the flake and the polarization angle indication. c) Polar maps of the intensity of Raman peaks at 256, 233, and 224 cm^{-1}, which correspond to A_g^1, B_{2g}, and A_g^1 modes of b-$As_{0.83}P_{0.17}$, showing clear polarization-dependent Raman intensities. The excitation laser wavelength is 532 nm and the laser size is around 1 μm.

the peaks gradually shift toward medium and high frequency regimes (Figure 4a).

In the b-AsP materials, several different bonds may exist including arsenic–arsenic, phosphorus–phosphorus, and arsenic–phosphorus. Therefore, it is reasonable that b-AsP would exhibit more Raman peaks than pure b-P or b-As, as Raman scattering probes a range corresponding to second or further neighbors and is sensitive to the short-range order beyond the nearest neighbors. In general, we expect a defined separation of the homoatomic arsenic–arsenic and phosphorus–phosphorus peaks and the heteroatomic arsenic–phosphorus peaks in the spectra. The homoatomic phosphorus–phosphorus peaks in b-P are located in the spectral region larger than 380 cm^{-1}. Homoatomic arsenic–arsenic peaks can be found in the region below 300 cm^{-1}. Raman studies on b-As_xP_{1-x} flakes with different x values reveal that for materials with high content of phosphorus, the characteristic peaks from b-P largely remain similar, except a slight redshift of the b-P peaks (Figure 4a). This finding is in accordance with the increasing amount of phosphorus–phosphorus bonds and the decreasing contribution of arsenic–arsenic bonds, as well as the change in bond strength and bond lengths in the system upon substitution. With increasing arsenic concentration, the phosphorus–phosphorus peaks gradually become weaker and weaker, and new arsenic–phosphorus peaks appear in the middle frequency regime and arsenic–arsenic peaks appear in the low frequency regime (Figure 4a). We also calculated the Raman spectra of b-AsP systems and found that the phosphorus–arsenic peaks are predicted to occur in the range from 300 to 380 cm^{-1} (Figure S7 and Table S2, Supporting Information), showing good agreement with the experimental observations.

Now let us focus on the polarization behavior of these Raman peaks. Figure 4b presents the polarization-resolved Raman spectra of a b-$As_{0.83}P_{0.17}$ flake at different incident laser polarization angles. A clear polarization dependence of the Raman behavior is observed, further confirming the anisotropic properties of these b-AsP materials as revealed from infrared absorption studies. The three major peaks (located at 256, 233, and 224 cm^{-1}) show polarization-dependent Raman intensity, as exhibited in Figure 4c. The observed angle-dependent Raman intensities are related to the structure of Raman tensors for each peak. Via these polarization-resolved Raman experiments, we found the following (see Figure S6, Supporting Information, and Figure 4c): (i) The exfoliated thin b-AsP flakes (<5 nm) are still crystalline since they exhibit similar Raman features with the bulk, (ii) Raman spectra from thick (>20 nm) and thin (<5 nm) flakes show similar characteristics in terms of the number of peaks, peak frequency, and peak–peak distance, (iii) there is no noticeable shift in the peak frequency for spectra collected at different incident laser polarization angles, and (iv) the maximum intensities for different peaks appear at different polarization angles, which is an indication of significant differences in their Raman tensors. We have performed polarization-resolved Raman studies on seven flakes and they show consistent polarization-dependent Raman intensity phenomena.

In conclusion, we have introduced a new family of layered semiconducting materials, black arsenic–phosphorus (b-As_xP_{1-x}). We show that these layered materials can be

rationally synthesized with highly tunable chemical compositions and can be exfoliated down to a few atomic layers. Electron transport measurements reveal the semiconducting nature of these materials. Through infrared absorption studies, we demonstrate that these layered b-AsP materials are semiconductors with tunable electronic and optical properties, via tuning the chemical compositions during material synthesis. Noticeably, this family of b-AsP materials fills up an interesting and technologically important gap in the LWIR regime in the electromagnetic spectra, which cannot be readily achieved by other 2D layered materials so far. Polarization-resolved infrared absorption and polarization-resolved Raman scattering studies reveal the in-plane anisotropic properties of these materials. Therefore, the layered b-AsP materials reported in this study contribute to the fabrication of functional devices based on all 2D layered materials. We envision that this family of new layered semiconductors with tunable band gaps in the LWIR regime, as well as with anisotropic properties, may find unique applications for electronic and optoelectronics devices operate at infrared regime.

Experimental Section

Synthesis of Composition-Tunable b-As_xP_{1-x}: b-As_xP_{1-x} samples with different nominal compositions were synthesized using a vapor transport method. Specifically, b-P (b-As_0P_1), b-$As_{0.25}P_{0.75}$, and b-$As_{0.4}P_{0.6}$ samples were prepared from a mixture of gray arsenic (Chempur, 99.9999%) and red phosphorus (Chempur, 99.999$^+$%) with molar ratio of 0:1, 1:3, and 2:3, respectively. Tin/tin (IV) iodide (Sn/SnI_4 = 10/5 mg per 250 mg batch) were added to the starting materials and acted as mineralizer additives to allow phase formation and crystal growth. All chemicals were enclosed in evacuated silica glass ampoules (length: 100 mm; inner diameter: 8 mm) during the reaction.

Synthesis of b-P and b-$As_{0.25}P_{0.75}$ samples was performed in a Nabertherm furnace (L3/11/P330). The following heating program was applied. (i) Heating the starting materials up to 650 °C within 8 h and holding for 5 h at this temperature, (ii) cooling down to 550 °C within 7.5 h and holding for 6 h at this temperature, (iii) further cooling down to 500 °C and holding for 8 h at this temperature, and (IV) cooling down to room temperature within 20 h. The b-$As_{0.4}P_{0.6}$ samples were synthesized using a Nabertherm furnace (L3/11/P320) and the heating program was changed to: (i) heating to 550 °C within 8 h and holding for 6 h at this temperature, (ii) cooling down to 500 °C within 2 h and holding for 8 h at this temperature, and (iii) cooling down to room temperature within 20 h.

The b-$As_{0.83}P_{0.17}$ samples were prepared from a mixture of gray arsenic (Chempur, 99.9999%) and red phosphorus (Chempur, 99.999$^+$%) and with a molar ratio 83:17. The mineralizing agent was lead (II) iodide (PbI_2, 12 mg per 625 mg batch). The chemicals were enclosed in evacuated silica glass ampoules during reaction (length: 100 mm, inner diameter: 10 mm). Synthesis was performed in a Nabertherm furnace (L3/11/P330). The following heating program was applied: (i) heating up to 550 °C within 8 h and holding for 84 h at this temperature and (ii) cooling down to room temperature within 20 h.

After synthesis, bulk b-AsP samples were mechanically exfoliated into flakes using a Scotch tape for optical and electrical measurements.

b-AsP Characterization: The AFM studies were performed using a Digital Instrument Dimensional 3100 AFM in tapping mode. We found that thin b-AsP flakes, similar to b-P samples, experience degradation when exposed to air. For b-AsP flakes covered with poly(methyl methacrylate (PMMA) layer or stored in argon glove box, they were stable and no noticeable degradation was observed over several month periods (Figure S8, Supporting Information).

Caution: In the case of handling b-AsP in oxygen or humid atmosphere, the formation of As_2O_3, which represents one of the major toxic components in the system, cannot be fully suppressed. Consequently, cautions should be taken when handling this material.

Device Fabrication and Measurements: Back-gate b-AsP FETs were fabricated using e-beam lithography. The metal contact was Ti/Au with thicknesses of 1/50 nm or 5/50 nm. The device measurements were performed using Agilent 4156B semiconductor parameter analyzer under two-terminal configuration in ambient condition.

Polarized Infrared Absorption Studies: Polarization-resolved infrared spectroscopic studies were performed in the 600–6000 cm^{-1} range using a Bruker optics Fourier transfer infrared spectrometer (Vertex 70) integrated with a Hyperion 2000 microscope system. The polarization angle of the incident light was adjusted using an infrared polarizer with an angle step of 15° or 30°. A 36x objective was used to collect the signal and the beam size was around 35 μm. The experiments were done in ambient condition.

Polarized Raman Studies: Polarization-resolved Raman studies were performed using a Renishaw micro Raman system with an excitation laser wavelength of 532 nm and beam size of ≈1 μm. The laser incident from *z*-direction and was linearly polarized in the *x*–*y* plane. The polarization direction of the laser was adjusted using a half-wavelength plate with an angle step of 15°. The detection was along the *z*-direction and was unpolarized. The samples were loaded into a vacuum chamber, and the laser power was kept around 5 μW to avoid sample degradation during Raman measurements. The spectrum integration time was 60 s. No obvious degradation of b-AsP was observed after a series of Raman measurements in vacuum.

DFT Calculations: First principles calculations were performed within the framework of DFT with Generalized Gradient Approximation-Perdew-Burke-Ernzerhof (GGA-PBE) functionals and Grimme D2 corrections for van der Waals interactions, to calculate the band gap and vibrational properties of b-AsP system. More details of the calculations are shown in the Supporting Information.

Supporting Information

Supporting Information is available from the Wiley Online Library or from the author.

Acknowledgements

B.L. and C.Z. conceived the idea. B.L., C.Z, and T.N. initiated the study. M.K. prepared black arsenic–phosphorus samples under supervision of T.N. X.W., Q.G., Y.J., F.X., H.W., and B.L. performed polarization-resolved IR absorption measurements and analysis. B.L., R.D., and S.B.C. performed polarization-resolved Raman studies and analysis. R.W., F.B., and F.P. performed the DFT simulations. B.L. and A.N.A. fabricated transistors and did the measurements. M.G. involved in discussion and schematic drawing. X.F. conducted the EDX measurements. B.L., M.K., T.N., C.Z., and R.W. wrote the paper with feedback from all others. The authors acknowledge Feng Wang and Jonghwan Kim of UC Berkeley for helpful discussions. The work at University of Southern California was supported by the Office of Naval Research (ONR) and the Air Force Office of Scientific Research (AFOSR). The authors would like to acknowledge the collaboration of this research with King Abdul-Aziz City for Science and Technology (KACST) via The Center of Excellence for Nanotechnologies (CEGN). The work at Technische Universität München (TUM) and Universität Regensburg was supported by the Deutsche Forschungsgemeinschaft (DFG) within the priority research program 1415. M.K. would like to thank the TUM Graduate School for support.

Received: April 14, 2015
Revised: May 12, 2015
Published online:

DOI: 10.1002/adma.201501758

[1] K. S. Novoselov, A. K. Geim, S. V. Morozov, D. Jiang, Y. Zhang, S. V. Dubonos, I. V. Grigorieva, A. A. Firsov, *Science* **2004**, *306*, 666.
[2] K. S. Novoselov, A. K. Geim, S. V. Morozov, D. Jiang, M. I. Katsnelson, I. V. Grigorieva, S. V. Dubonos, A. A. Firsov, *Nature* **2005**, *438*, 197.
[3] Y. B. Zhang, Y. W. Tan, H. L. Stormer, P. Kim, *Nature* **2005**, *438*, 201.
[4] K. S. Novoselov, D. Jiang, F. Schedin, T. J. Booth, V. V. Khotkevich, S. V. Morozov, A. K. Geim, *Proc. Natl. Acad. Sci. USA* **2005**, *102*, 10451.
[5] J. N. Coleman, M. Lotya, A. O'Neill, S. D. Bergin, P. J. King, U. Khan, K. Young, A. Gaucher, S. De, R. J. Smith, I. V. Shvets, S. K. Arora, G. Stanton, H. Y. Kim, K. Lee, G. T. Kim, G. S. Duesberg, T. Hallam, J. J. Boland, J. J. Wang, J. F. Donegan, J. C. Grunlan, G. Moriarty, A. Shmeliov, R. J. Nicholls, J. M. Perkins, E. M. Grieveson, K. Theuwissen, D. W. McComb, P. D. Nellist, V. Nicolosi, *Science* **2011**, *331*, 568.
[6] Z. Liu, L. Ma, G. Shi, W. Zhou, Y. Gong, S. Lei, X. Yang, J. Zhang, J. Yu, K. P. Hackenberg, A. Babakhani, J. C. Idrobo, R. Vajtai, J. Lou, P. M. Ajayan, *Nat. Nanotechnol.* **2013**, *8*, 119.
[7] L. Chen, B. Liu, A. Abbas, Y. Ma, X. Fang, Y. Liu, C. Zhou, *ACS Nano* **2014**, *8*, 11543.
[8] B. Radisavljevic, A. Radenovic, J. Brivio, V. Giacometti, A. Kis, *Nat. Nanotechnol.* **2011**, *6*, 147.
[9] A. Splendiani, L. Sun, Y. B. Zhang, T. S. Li, J. Kim, C. Y. Chim, G. Galli, F. Wang, *Nano Lett.* **2010**, *10*, 1271.
[10] Y. Zhang, T. R. Chang, B. Zhou, Y. T. Cui, H. Yan, Z. K. Liu, F. Schmitt, J. Lee, R. Moore, Y. L. Chen, H. Lin, H. T. Jeng, S. K. Mo, Z. Hussain, A. Bansil, Z. X. Shen, *Nat. Nanotechnol.* **2014**, *9*, 111.
[11] S. Najmaei, Z. Liu, W. Zhou, X. L. Zou, G. Shi, S. D. Lei, B. I. Yakobson, J. C. Idrobo, P. M. Ajayan, J. Lou, *Nat. Mater.* **2013**, *12*, 754.
[12] B. Liu, L. Chen, G. Liu, A. Abbas, M. Fathi, C. Zhou, *ACS Nano* **2014**, *8*, 5, 5304.
[13] L. Li, Y. Yu, G. J. Ye, Q. Ge, X. Ou, H. Wu, D. Feng, X. H. Chen, Y. Zhang, *Nat. Nanotechnol.* **2014**, *9*, 372.
[14] H. Liu, A. T. Neal, Z. Zhu, Z. Luo, X. F. Xu, D. Tomanek, P. D. D. Ye, *ACS Nano* **2014**, *8*, 4033.
[15] F. Xia, H. Wang, Y. Jia, *Nat. Commun.* **2014**, *5*, 4458.
[16] S. P. Koenig, R. A. Doganov, H. Schmidt, A. H. C. Neto, B. Ozyilmaz, *Appl. Phys. Lett.* **2014**, *104*.
[17] M. Köpf, N. Eckstein, D. Pfister, C. Grotz, I. Krüger, M. Greiwe, T. Hansen, H. Kohlmann, T. Nilges, *J. Cryst. Growth* **2014**, *405*, 6.
[18] A. Abbas, B. Liu, L. Chen, Y. Ma, S. Cong, N. Aroonyadet, M. Köpf, T. Nilges, C. Zhou, *ACS Nano* **2015**, *9*, 5618.
[19] Z. Yang, J. Hao, S. Yuan, S. Lin, H. M. Yau, J. Dai, S. P. Lau, *Adv. Mater.* **2015**, *DOI:10.1002/adma.201500990.*
[20] Y. Zhang, T. T. Tang, C. Girit, Z. Hao, M. C. Martin, A. Zettl, M. F. Crommie, Y. R. Shen, F. Wang, *Nature* **2009**, *459*, 820.
[21] Q. H. Wang, K. Kalantar-Zadeh, A. Kis, J. N. Coleman, M. S. Strano, *Nat. Nanotechnol.* **2012**, *7*, 699.
[22] K. F. Mak, C. Lee, J. Hone, J. Shan, T. F. Heinz, *Phys. Rev. Lett.* **2010**, *105*, 136805.
[23] Y. Gong, Z. Liu, A. R. Lupini, G. Shi, J. Lin, S. Najmaei, Z. Lin, A. L. Elias, A. Berkdemir, G. You, H. Terrones, M. Terrones, R. Vajtai, S. T. Pantelides, S. J. Pennycook, J. Lou, W. Zhou, P. M. Ajayan, *Nano Lett.* **2014**, *14*, 442.
[24] S. B. Desai, G. Seol, J. S. Kang, H. Fang, C. Battaglia, R. Kapadia, J. W. Ager, J. Guo, A. Javey, *Nano Lett.* **2014**, *14*, 4592.
[25] Q. Feng, Y. Zhu, J. Hong, M. Zhang, W. Duan, N. Mao, J. Wu, H. Xu, F. Dong, F. Lin, C. Jin, C. Wang, J. Zhang, L. Xie, *Adv. Mater.* **2014**, *26*, 2648.
[26] H. L. Li, X. D. Duan, X. P. Wu, X. J. Zhuang, H. Zhou, Q. L. Zhang, X. L. Zhu, W. Hu, P. Y. Ren, P. F. Guo, L. Ma, X. P. Fan, X. X. Wang, J. Y. Xu, A. L. Pan, X. F. Duan, *J. Am. Chem. Soc.* **2014**, *136*, 3756.
[27] X. M. Wang, A. M. Jones, K. L. Seyler, V. Tran, Y. C. Jia, H. Zhao, H. Wang, L. Yang, X. D. Xu, F. N. Xia, *Nat. Nanotechnol.* **2015**, *DOI:10.1038/nnano.2015.71.*
[28] I. Shirotani, J. Mikami, T. Adachi, Y. Katayama, K. Tsuji, H. Kawamura, O. Shimomura, T. Nakajima, *Phys. Rev. B* **1994**, *50*, 16274.
[29] S. Lange, M. Bawohl, R. Weihrich, T. Nilges, *Angew. Chem. Int. Ed.* **2008**, *47*, 5654.
[30] O. Osters, T. Nilges, F. Bachhuber, F. Pielnhofer, R. Weihrich, M. Schoneich, P. Schmidt, *Angew. Chem. Int. Ed.* **2012**, *51*, 2994.
[31] T. Nilges, M. Kersting, T. Pfeifer, *J. Solid State Chem.* **2008**, *181*, 1707.
[32] S. Lange, P. Schmidt, T. Nilges, *Inorg. Chem.* **2007**, *46*, 4028.
[33] Z. Y. Zhang, J. F. Xie, D. Z. Yang, Y. H. Wang, M. S. Si, D. S. Xue, *Appl. Phys. Express* **2014**, *8*, 055201.